AAS 13-309

PRELIMINARY STATISTICAL TRAJECTORY AND ATMOSPHERE RECONSTRUCTION OF MSL ENTRY, DESCENT, AND LANDING

Soumyo Dutta* **and Robert D. Braun†**

On August 5, 2012, the Mars Science Laboratory spacecraft landed the heaviest payload on Mars using the largest aeroshell and supersonic parachute ever used by a planetary entry mission. Moreover, an innovative Sky Crane landing system was utilized to softly and accurately place the science payload on the ground near the desired target. The spacecraft recorded inertial measurement unit data and radar altimeter measurements during its descent through the Martian atmosphere and the aeroshell was also instrumented with flush atmospheric data system sensors that allow for the reconstruction of the vehicle's pressure distribution and freestream atmospheric conditions. This paper shows the preliminary results of the vehicle's trajectory and atmosphere reconstruction using a statistical estimation methodology that utilizes an extended Kalman filter. This method has been demonstrated with simulated Mars entry data in the past, and has the capability of simultaneously estimating the parameters and their uncertainties using the initial state covariance and measurement uncertainties.

INTRODUCTION

The Mars Science Laboratory (MSL) successfully landed on Mars on Aug. 5, 2012. The vehicle became the seventh, successful U.S. vehicle to complete entry, descent, and landing (EDL) on Mars and pushed the boundaries of current EDL technology.[1] The vehicle landed at the near-equatorial Gale Crater that is at an altitude of about -4.5 km, although the spacecraft was designed to land at $\pm 45^\circ$ latitude and +1 km altitude.[2]

The spacecraft contained on-board sensors like 3-axis accelerometers, 3-axis gyroscopes, and radar altimeter that guided the vehicle during EDL. Additionally, the recorded data allow engineers to reconstruct the vehicle's path and the atmosphere it encountered after the fact. Moreover, MSL was also carrying an innovative aeroshell-mounted instrumentation suite, named the MSL EDL Instrumentation (MEDLI),[3] that recorded pressure measurements on the surface of the aeroshell using a flush atmospheric data system (FADS) and took in-depth temperature measurements throughout the heatshield for a large time period of the entry phase. Together, this dataset provides enough independent measurements to characterize the spacecraft's trajectory, atmosphere, and aerodynamic characteristics. If statistical estimation algorithms that incorporate information about the initial state uncertainties and measurement uncertainties are applied during the reconstruction process, one can also quantify the uncertainties of the estimated parameters.

*Graduate Research Assistant, Daniel Guggenheim School of Aerospace Engineering, Georgia Institute of Technology, 270 Ferst Drive, Atlanta, GA, Email: soumyo.dutta@gatech.edu.

†David and Andrew Lewis Professor of Space Technology, Daniel Guggenheim School of Aerospace Engineering, Georgia Institute of Technology, 270 Ferst Drive, Atlanta, GA.

The novel feature about the MEDLI data is that it makes atmospheric parameters observable without assuming *perfect* knowledge of the aerodynamic properties, something that was not a luxury for most past Mars EDL that were not equipped with FADS sensors. Without FADS, accelerometer data are the only means on estimating atmospheric quantities after the trajectory has been reconstructed. However, since the prediction equations for the accelerometer measurements are also a function of aerodynamic parameters, one has to assume complete knowledge of aerodynamics to reduce the problem to an one-equation-one-unknown-type of analysis. The necessity of assuming that the aerodynamic parameters are known *perfectly* for atmospheric reconstruction leads to a confounding of aerodynamic and atmospheric uncertainties.

Due to the disparate measurement types present in the MSL flight dataset, a comprehensive methodology is needed to utilize all of the data types to estimate as many relevant parameters, while also characterizing the parameters' uncertainties. The authors have demonstrated such a methodology in the past on simulated MSL-type datasets[4] and recent flight data from Mars Pathfinder,[5] Mars Exploration Rovers,[6] and the Phoenix lander.[7] The same methodology is implemented here on the MSL dataset for a preliminary reconstruction of the spacecraft's trajectory and atmosphere. Aerodynamic parameter reconstruction has been excluded in the current paper and will be demonstrated in future work.

The paper provides a background about the MSL mission and the MEDLI instrumentation. Next, the data collected on-board and used in the reconstruction is presented followed by a discussion on the reconstruction methodology itself, including the equations of motion, measurement equations, and the algorithm for the statistical estimators. Finally, the results of the trajectory and atmosphere reconstruction are presented and discussed.

MARS SCIENCE LABORATORY

MSL used a 4.5 m diameter, 70-deg. sphere-cone aeroshell that reached the limit of current launch vehicle fairing diameters.[1] The vehicle also utilized a 19.8 m diameter Disk-gap Band (DGB) supersonic parachute,[8] which reached the limit of available test data for such parachutes.[9] Additionally, the landed mass for MSL was around 900 kg, which was 5 times the landed mass of the previous largest rovers landed on Mars. Finally, the EDL system was designed to land MSL within a 25 km $\times$ 20 km ellipse, a much smaller landing footprint than any previous Mars entry spacecraft.[10] To accomplish so many unique and challenging firsts, MSL utilized a hypersonic guidance scheme and used an innovative Sky Crane landing system to drop-off the rover softly on the Martian surface. These innovative aspects of MSL's operations can be seen in Fig. 1.[1]

Mars Science Laboratory Entry, Descent, and Landing Instrumentation

The MEDLI sensor suite on-board MSL took in-situ measurements of the pressure and temperature distribution on the aeroshell. It consisted of two instruments: Mars Entry Atmospheric Data System (MEADS) - a FADS sensor - to take the pressure measurements and MEDLI Integrated Sensor Plug (MISP) to take the aerothermodynamic data within the width of the aeroshell.[3] Since only MEADS data aids trajectory and atmosphere reconstruction, the processing of temperature data from the MISP sensors is not covered in this paper.

MEADS's science objective is to reconstruct the atmospheric properties within certain bounds when the dynamic pressure is greater than 850 Pa. Freestream dynamic pressure (q_∞) is to be estimated within $\pm 2\%$ and angle of attack (α) and sideslip angle (β) are to be reconstructed within

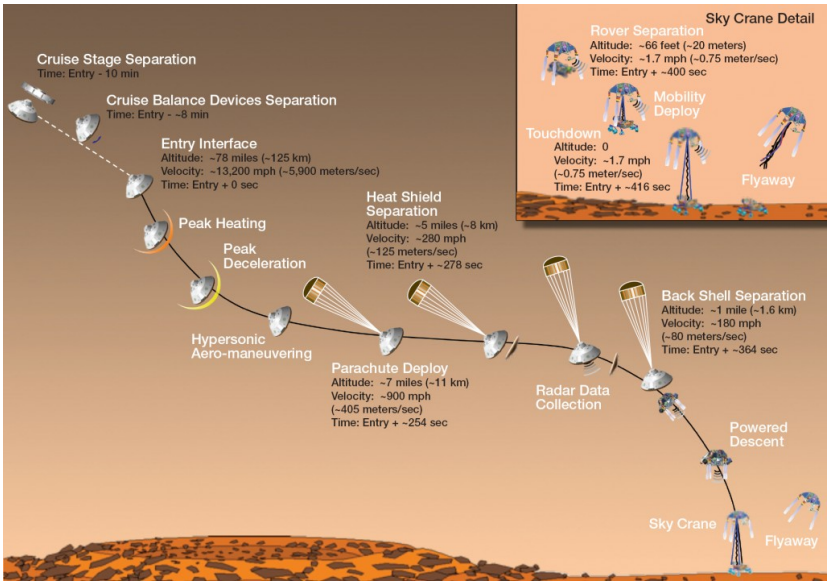

Figure 1. Mars Science Laboratory entry, descent, and landing sequence.[11]

± 0.5 deg.[12] Additionally, the MEADS transducers are expected to provide surface pressure measurements to reconstruct the overall pressure distribution on the aeroshell. In order to achieve all of these targets, MEADS collects pressure data from seven pressure transducers located around the forebody of the aeroshell (see Fig. 2).

The locations of the transducers are based on the predicted pressure distribution on the aeroshell. It is expected from the nominal trajectory that the stagnation pressure is to be around transducers P1 and P2, while P4, P6, and P7 serve as the transducers that will help reconstruct the sideslip angle. All of the transducers besides P6 and P7 are expected to help reconstruct the angle of attack history.[3]

Collected Data

The data collected on-board MSL consists of inertial measurement unit (IMU) observations (3-axis accelerometers and 3-axis gyroscopes), radar altimeter data, and the MEADS measurements. These data were used in the reconstruction process and are presented below. Entry interface (EI) was reported at a Spacecraft Clock Time (SCLK) of 397501714.953130 s and data was first collected at SCLK of 397501174.997338 s.[14,15] The data presented below have been adjusted from SCLK to an epoch where entry interface is zero.

Inertial Measurement Unit Data The raw data collected on-board MSL consisted of δV and $\delta\theta$ measurements that were converted into accelerations and angular rates using finite differencing. The nominal sampling rate of the data was 200 Hz. Although the vehicle contained two sets of IMUs, only data from IMU-A were during EDL by the flight controller. The reference frame for the IMU was different from typical flight dynamics convention of the body frame. The IMU frame, also referred as the Descent Stage (DS) frame, had its positive z-direction outwards in the vehicle axial direction, while the x-direction is in the pitch plane. A negative 90 deg. rotation in the y-direction brought the DS frame to the flight dynamics conventional body frame.[14] Figure 3 shows the unfiltered accelerations and angular rates in the vehicle body frame. This data was used in its

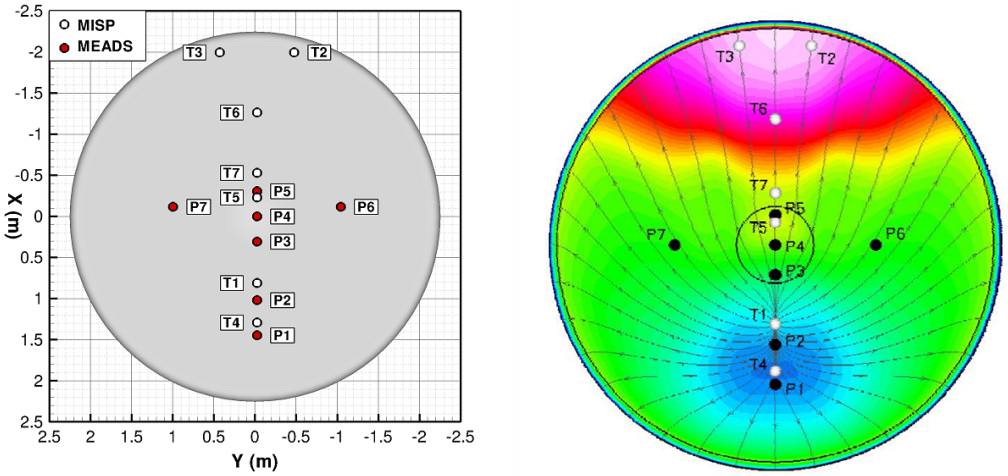

(a) MEDLI locations[13]

(b) Predicted flow over the aeroshell.[3]

Figure 2. MEDLI sensors.

unfiltered form for the reconstruction.

Terminal Descent Sensor - Radar Altimeter Data The radar altimeter took measurements during the terminal descent stage of the trajectory. The sensor suite consisted of several radar altimeters which collected range and range rate information. This data was processed on-board the vehicle to calculate a slant range and slant velocity. For this analysis, the slant range information was used for the trajectory reconstruction. The unfiltered 20 Hz data and the down-sampled 1 Hz data are shown in Fig. 4. Also shown is the slant range uncertainty calculated by the on-board flight software and this uncertainty was used as the measurement noise covariance in the analysis.

Mars Entry Atmospheric Data System MEADS started collecting data from cruise stage separation at a nominal sampling rate of 8 Hz. The data was converted to engineering units using pre-flight and cruise-stage calibration data and an in-flight zero applied to the data.[15] Data was collected until shortly before the parachute mortar fire; however, the optimal calibration of the MEADS data was only guaranteed when the dynamic pressure was greater than 850 Pa. For MSL, this range fell between 50 and 175 s after EI. Only data from this restricted region is used for the analysis, although the data shown below in Figs. 5 are for all times after EI. The data was found to be close to the expected values and very little discrepancy was noticed in the initial analysis.[15]

RECONSTRUCTION METHODOLOGY

Statistical estimation techniques similar to this methodology has been used recently for planetary entry vehicle flight reconstruction.[15,16] However, most of these analyses have used the accelerometer measurements in the process equations to propagate the velocity vector. The process equations for these methods are thus similar to the equations used by deterministic reconstructions used in the past. On the other hand, the process equations in this paper use lift and drag coefficients estimated with the current state vector to propagate the velocity vector, thus precluding the need of accelerometer data to propagate the state vector. This also allows for the accelerometer observations to be treated as measurements by the estimation methodology. Since accelerations are a function of the sensed force on a body, which in turn depends on the freestream density and velocity, treat-

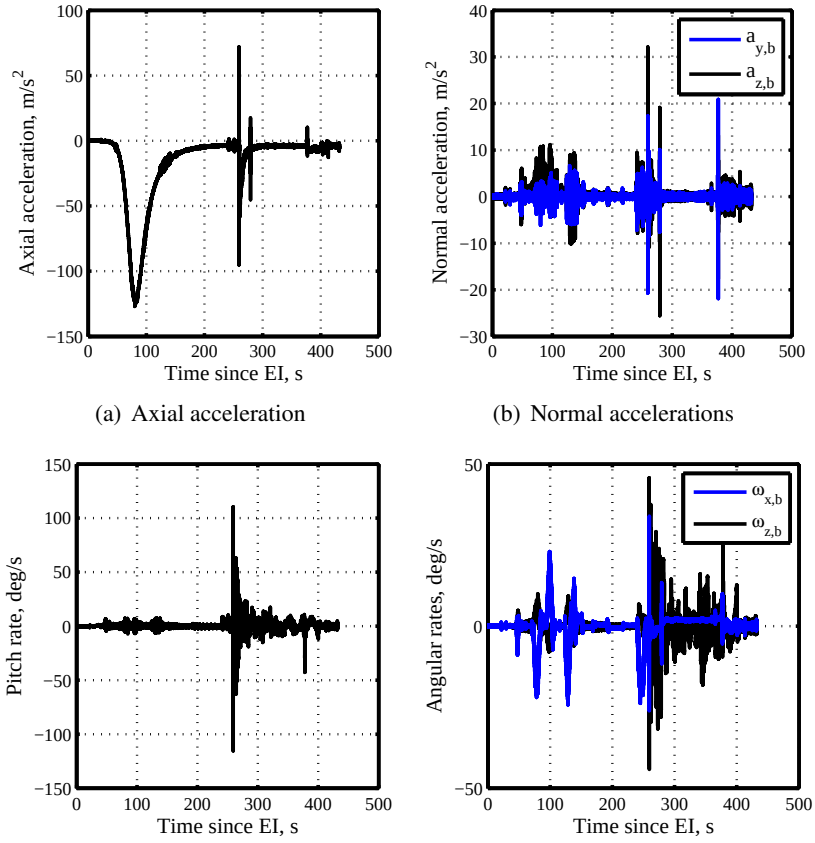

(a) Axial acceleration (b) Normal accelerations

(c) Pitch rate (d) Roll and Yaw rates

Figure 3. MSL inertial measurement unit data.

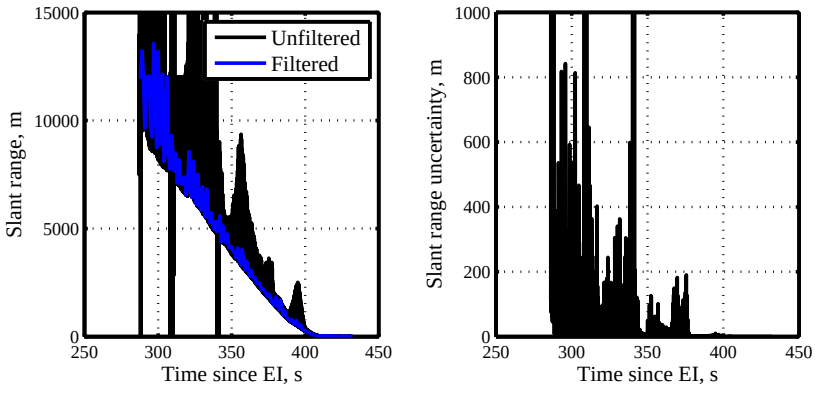

(a) Slant range (b) Slant range uncertainty

Figure 4. MSL terminal descent sensor slant range and uncertainty.

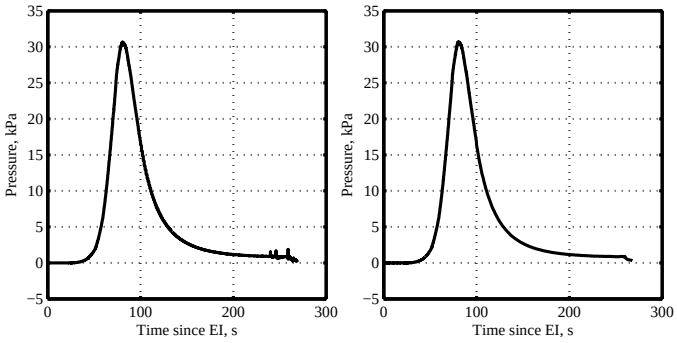

(a) Pressure port 1

(b) Pressure port 2

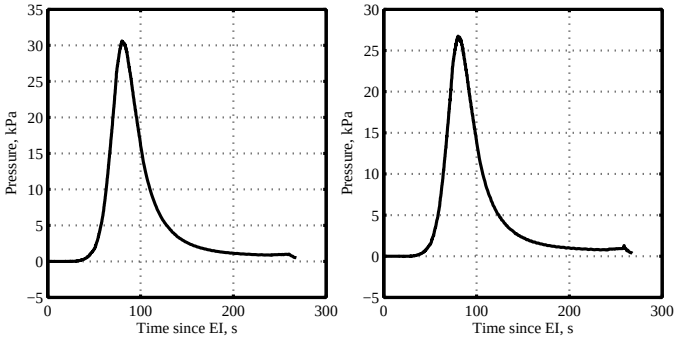

(c) Pressure port 3

(d) Pressure port 4

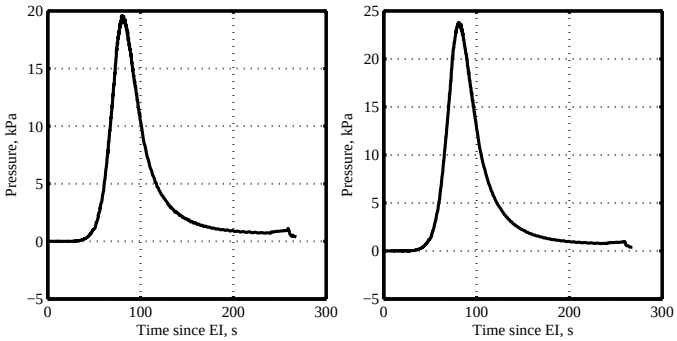

(e) Pressure port 5

(f) Pressure port 6

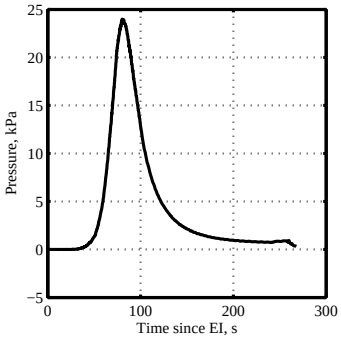

(g) Pressure port 7

Figure 5. MEADS data for pressure ports 1-7.

ing accelerometer data as measurements provides an additional source of measurements with which atmospheric parameters can be directly estimated in addition to FADS measurements.

The methodology used for reconstructing Mars EDL vehicle flight parameters consists of three parts: the process equations, the estimation method, and the measurement equations. The estimation method used for the current study is the extended Kalman filter (EKF), which has long been regarded as the standard in the field of signal processing. The estimator is guided by the process equations, which describe the system dynamics of the problem, and the measurement equations of the various data types being used to inversely estimate the parameters of interest. The process equations are of the form shown in Eq. (1a), where the function f is a non-linear dynamic equation of the state vector, $\mathbf{x}$, and in the case of EDL trajectories f consists of the equations of motion described in the next section (Eqs. (2)). The state noise (also called the process noise) vector is defined as $\mathbf{w}$, which is *usually* assumed to be a time-varying, Gaussian white noise. The measurement ($\mathbf{y}$) vector (Eq. (1b)) is also a nonlinear function of the state vector (in this case represented by h) and a measurement noise vector ($\mathbf{v}$) that is also a time-varying, Gaussian white noise. The Gaussian distribution assumption is common to many types of estimation methods, although there is no requirement of it from the perspective of estimation and information theory.

$$\dot{\mathbf{x}} = f\left(t, \mathbf{x}, \mathrm{w}\left(t\right)\right) \tag{1a}$$

$$\mathbf{y} = h\left(t, \mathbf{x}, \mathbf{v}\left(t\right)\right) \tag{1b}$$

Process Equations

The estimators need dynamic equations of motion, as seen in Eqs. (2), to propagate the estimate of the states in time. The state vector consists of vehicle's position, velocity, attitude, freestream pressure (P_∞), and freestream density (ρ_∞) - the latter two included to capture time-varying aerodynamic states. The equations of motion use the estimated states at a previous time to create a nominal estimate of the state at the present time.

The equations presented here are an amalgamation from several sources.[17,18,16] The position is in terms of planet-centric radius (r), latitude (ϕ), and longitude (θ), while the velocity magnitude (V), flight path angle (γ), and heading angle (ψ) are defined relative to the planet surface.[17] Note that the heading angle is defined in the horizontal plane where due East is 0° and due North is 90°. The attitude states are given in terms of a quaternion between the inertial (J2000) and body frame (q_0, q_1, q_2, q_3) and another quaternion between the inertial (J2000) and the planet-centric, planet-fixed frame (e_0, e_1, e_2, e_3). Knowledge of the two quaternions with respect to the inertial frame provides enough information to calculate the orientation between the vehicle-carried local horizontal frame and the body frame,[18] which is needed to predict the lift and drag coefficients.

The intermediate states and parameters needed to define the equations of motion include the planetary rotation rate (ω), the angular rates in the body frame (ω_x, ω_y, and ω_z) that come from the on-board gyroscopes, and the altitude-dependent gravitational acceleration (g) based on a J2 mass distribution model.

The aerodynamic parameters are found using look-up tables based on the work by Dyakonov et al.[19] F_N and F_T represent the normal (lift) and tangential (drag) forces in the body axis and bank angle (ν) is used for lift modulation.

The dynamical equations for the freestream pressure and density are derived from the hydrostatic equation and the perfect gas law and the derivation is described in the work of Karlgaard et al.[16]

and Dutta and Braun.[20] Eqs. (2g) and (2h) use an isothermal assumption that is valid over small changes in the altitude. Since the freestream pressure and density rate equations are used as process equations and are propagated over small time steps, this assumption is reasonable. Note that the process noise chosen for the reconstruction process is tuned to compensate for potential issues with these equations.

$$\dot{r} = V \sin\gamma \tag{2a}$$

$$\dot{\phi} = \frac{V \cos\gamma \sin\psi}{r} \tag{2b}$$

$$\dot{\theta} = \frac{V \cos\gamma \cos\psi}{r \cos\phi} \tag{2c}$$

$$\dot{V} = \frac{F_T}{m} - g \sin\gamma + \omega^2 r \cos\phi \left(\sin\gamma \cos\phi - \cos\gamma \sin\phi \sin\psi\right) \tag{2d}$$

$$\begin{aligned}\dot{\gamma} = \frac{1}{V}\Bigg[&\frac{F_N \cos\nu}{m} - g\cos\gamma + \frac{V^2}{r}\cos\gamma + 2\omega V \cos\phi\cos\psi \\ &+\omega^2 r \cos\phi \left(\cos\gamma\cos\phi + \sin\gamma\sin\phi\sin\psi\right)\Big]\end{aligned} \tag{2e}$$

$$\begin{aligned}\dot{\psi} = \frac{1}{V}\Bigg[&\frac{F_N \sin\nu}{m\cos\gamma} - \frac{V^2}{r}\cos\gamma\cos\psi\tan\phi + 2\omega V\left(\tan\gamma\cos\phi\sin\psi - \sin\phi\right) \\ &-\frac{\omega^2 r}{\cos\gamma}\sin\phi\cos\phi\cos\psi\Bigg]\end{aligned} \tag{2f}$$

$$\dot{P_\infty} = -\rho_\infty g V \sin\gamma \tag{2g}$$

$$\dot{\rho_\infty} = -\frac{\rho_\infty^2 g V \sin\gamma}{P_\infty} \tag{2h}$$

$$\begin{bmatrix} \dot{q_0} \\ \dot{q_1} \\ \dot{q_2} \\ \dot{q_3} \end{bmatrix} = \frac{1}{2}\begin{bmatrix} -q_1 & -q_2 & -q_3 \\ q_0 & -q_3 & q_2 \\ q_3 & q_0 & -q_1 \\ -q_2 & q_1 & q_0 \end{bmatrix}\begin{bmatrix} \omega_x \\ \omega_y \\ \omega_z \end{bmatrix} \tag{2i}$$

$$\begin{bmatrix} \dot{e_0} \\ \dot{e_1} \\ \dot{e_2} \\ \dot{e_3} \end{bmatrix} = \frac{1}{2}\begin{bmatrix} -e_1 & -e_2 & -e_3 \\ e_0 & -e_3 & e_2 \\ e_3 & e_0 & -e_1 \\ -e_2 & e_1 & e_0 \end{bmatrix}\begin{bmatrix} 0 \\ 0 \\ \omega \end{bmatrix} \tag{2j}$$

Extended Kalman Filter

Extended Kalman filters have been extensively used in the past for Mars EDL reconstruction. The algorithm for this well-known filter is summarized below:[21,22]

1. Initialize the state vector and the state covariance matrix at time $t_{k-1} = t_0$ and let $k = 1$, where k is an index of the epoch when a measurement is first available.

2. Read in the measurement at time t_k.

3. Calculate a nominal state ($\hat{\mathbf{x}}_\mathbf{k}^-$) at time t_k by integrating the non-linear equations of motions with $\hat{\mathbf{x}}_{\mathbf{k-1}}^+$ as the initial condition.

4. Calculate the nominal state covariance matrix ($\hat{P}_k^-$) by integrating the Riccati equations (Eq. (3a)).

5. Calculate the measurement residual vector ($\mathbf{y_k}$), the measurement sensitivity matrix (H_k), and the Kalman gain (K_k) using the nominal state and state covariance (Eq. (3b)).

6. Calculate the best estimate of the state ($\hat{\mathbf{x}}_\mathbf{k}^+$) and covariance ($\hat{P}_k^+$) using Eqs. (3c) and (3d).

7. Increment counter k and go back to step 2 until measurements at all times have been processed.

$$\dot{P} = AP + P^T A^T + BQB^T \tag{3a}$$

$$K_k = \hat{P}_k^- H_k^T \left(H_k \hat{P}_k^- H_k^T + R_k \right)^{-1} \tag{3b}$$

$$\hat{\mathbf{x}}_k^+ = \hat{\mathbf{x}}_k^- + K_k \left(\mathbf{y_k} - \mathbf{h} \left(\hat{\mathbf{x}}_\mathbf{k}^- \right) \right) \tag{3c}$$

$$\hat{P}_k^+ = (I - K_k H_K) \hat{P}_k^- (I - K_k H_k)^T + K_k R_k K_k^T \tag{3d}$$

A is the Jacobian of the process equations with respect to the state vector, while B is the Jacobian of the process equations with respect to the state noise vector. The state noise vector for EDL reconstruction comes from uncertainties in the process equations, such as aerodynamic and atmospheric uncertainties. The matrix I in the covariance update equation is the identity matrix. The measurement covariance matrix (R) is defined at time k and information from sensor calibration is used in this matrix. The covariance of the state noise vector (Q) consists of noise variables in the process equations, such as the sensor uncertainty of the angular rate gyroscopes or tuning parameters for the velocity vector equations. Dutta et al.[4] discusses the values used for the state and measurement noise covariances.

Measurement Equations

Measurement equations are used to predict the measurement value based on the current estimate of the state. The actual measurements can then be compared with the predicted measurements, and the state can be appropriately updated. Most of the statistical estimators used in this work are based on linear filter theory, so the estimator assumes that the measurements are a linear function of the state vector plus a measurement error ($\mathbf{v}$) as described in Eq. 1b. For most measurement types, h is a non-linear function of the state vector, but using a first-order Taylor series expansion, Eq. (1b) can be linearized about a point (the nominal estimate of the state, $\bar{\mathbf{x}}$) as shown in Eq. (4), where $\tilde{\mathbf{x}}$ is the deviation in state from $\mathbf{x}$. A measurement sensitivity (Jacobian) matrix (H), shown in Eq. (5), is defined as

$$\mathbf{y_i} = \mathbf{h_i}(\bar{\mathbf{x}}) + [\partial \mathbf{h} / \partial \mathbf{x}]_{\mathbf{x}=\bar{\mathbf{x}}} \, \tilde{\mathbf{x}} + \mathbf{v_i} \tag{4}$$

$$H = \left[\begin{array}{c} \partial h_1 / \partial \mathbf{x} \\ \cdot \\ \partial h_n / \partial \mathbf{x} \end{array} \right]_{\mathbf{x}=\bar{\mathbf{x}}} \tag{5}$$

The measurement sensitivity equations have been developed for every measurement type included in the estimation process. Christian et al. discusses the development of the sensitivity matrix for

accelerometer and radar altimeter measurements.[23] More detailed expressions for the measurement sensitivity equations pertaining to accelerometer and radar altimeter measurements can also be found in the work of Karlgaard et al.[16]

For FADS sensors, the measurement equation has to predict the static pressure value at a specific transducer, where the static pressure value is a function of three parameters: total angle of attack (α_t), freestream Mach number (M_∞), and the orientation of the transducer on the aeroshell, which are given in terms clock angle (ζ) and cone angle (η).[20] During the hypersonic EDL phase, the velocity of the vehicle is large with respect to the wind velocity, so the planet-relative velocity can be used to calculate the angle of attack (α) and angle of sideslip (β). The two orientation angles can then be combined into a total angle of attack. Since the locations of the pressure measurement orifices are known, the pressure coefficient (C_p) at each orifice can then be found from tables created from the vehicle aerodynamic database. Dutta and Braun[20] present an example of such a look-up table. After the pressure coefficient is found, the pressure at each surface location can be predicted using the vehicle velocity and freestream density, which are part of the state vector.

Optimal Smoothing

The reconstruction can start from atmospheric entry (forward pass) or a projected landing location (backwards pass). The forward pass starts its estimate from an initial state and covariance that is found independent of the trajectory reconstruction process and the reconstruction is conducted in a chronological manner. The backwards pass has the advantage of starting at a smaller uncertainty value as it begins from the end of the forward estimate.

Due the advantage of both types of reconstructions, the forward and backward pass estimates (denoted by the subscripts f and b respectively) are often combined using the Fraser-Potter smoothing solution[24] to create a best estimated solution. This smoothing solution is shown in Eqs. (6). It is advantageous to combine both the forward and backward estimates in finding an optimal estimate of the trajectory.[16] The forward pass estimate at time k uses the measurement data from entry to k, while the backward pass estimate at k uses the measurement data from landing time to k. The combined smoothed estimate at time k will then use measurement data at all times to create the estimate at k and is similar to a batch least-squares solution.[25]

$$\hat{P}_k = \left[\hat{P}_{f,k}^{-1} + \hat{P}_{b,k}^{-1}\right]^{-1} \tag{6a}$$

$$\hat{\mathbf{x}}_k = \hat{P}_k \left[\hat{P}_{f,k}^{-1}\hat{\mathbf{x}}_{f,k} + \hat{P}_{b,k}^{-1}\hat{\mathbf{x}}_{b,k}\right]^{-1} \tag{6b}$$

RESULTS

With the EKF serving as the statistical estimation method, the MSL flight data presented in Sec. is reconstructed to provide the best estimate of the spacecraft's trajectory and Mars' atmosphere during EDL.

Initial Conditions

The results of the reconstruction below are shown for a time period starting at the entry interface and ending with touchdown. However, the data needed for the reconstruction were available at many different epochs. For example, IMU and MEADS data was available from cruise stage separation, while radar altimeter data was first available late into the descent phase. Additionally, the initial

Table 1. Initial Conditions for Mars Science Laboratory (at Entry Interface)

State	Condition	Standard Deviation (3σ)*
Radius (centric), m	3522199.99995045	32.0662
Latitude (centric), deg	-3.91864700387748	0.000781
Longitude (East), deg	126.718029798353	0.000367
Velocity (inertial), m/s	6083.32706805884	0.026059
Flight-path angle (inertial), deg	-15.4891541985927	0.000400
Azimuth angle (inertial), deg	93.2064558818444	0.000268
Freestream pressure, Pa†	2.972631067401E-4	$10P_{\infty,0}$
Freestream density, kg/m^2†	2.838149463198E-8	$10\rho_{\infty,0}$

*Calculated using Monte Carlo simulation starting with known covariance at EI - 9 min
†Determined by using a deterministic reconstruction

Table 2. Initial Conditions for Quaternions (at Entry Interface)

	q (J2000 to DS)	e (J2000 to MCMF)
Scalar	0.001821754603842	0.93190195328
i	0.401058954219038	0.16755447261
j	0.405863844667464	0.27063814466
k	-0.821232571194455	0.17389434385

Note: Initial Euler angle uncertainties assumed to be ± 0.2 deg

state estimate was available at three different epochs (EI - 9 min, 10 s; EI - 9 min; and EI) while the initial covariance was only available at EI - 9 min, 10 s. Thus, all of these values had to be brought to a standard starting epoch.

In order to find the initial conditions for all states and covariances at the entry interface, the statistical methodology described in the earlier section had to be preceded by a deterministic reconstruction. The deterministic reconstruction used the IMU data to propagate the vehicle position, velocity, and attitude from EI - 9 min to touchdown. This process is similar to what was used for several past Mars EDL reconstructions.[26,27,28] This deterministic reconstruction was also the source for initial estimate of freestream density and pressure. Freestream density was reconstructed using the IMU data and assuming the perfect knowledge of aerodynamic parameters, while the freestream pressure was found by integrating the hydrostatic equation with a surface pressure of 695 Pa that was measured by MSL shortly after it reached the Martian surface.[15] Although this procedure once again confounded aerodynamic and atmospheric uncertainties, one should note that the results from these reconstructions are only used to establish the *initial conditions* for freestream density and pressure at EI; afterwards, a statistical estimation method is used for the final reconstruction and this method uses both IMU and FADS data for atmosphere reconstruction, eliminating the need for assuming *perfect* knowledge of the aerodynamic parameters.

The initial conditions for MSL's state vector are summarized in Tables 1 and 2. The initial covariance at EI was found using Monte Carlo simulation with an initial state and covariance known at EI - 9 min, 10 s.

Trajectory Reconstruction

The reconstructed trajectory for MSL is shown in Fig. 6. Some major EDL events can be identified on the reconstructed profile and these have been labeled in the zoomed inset of the terminal

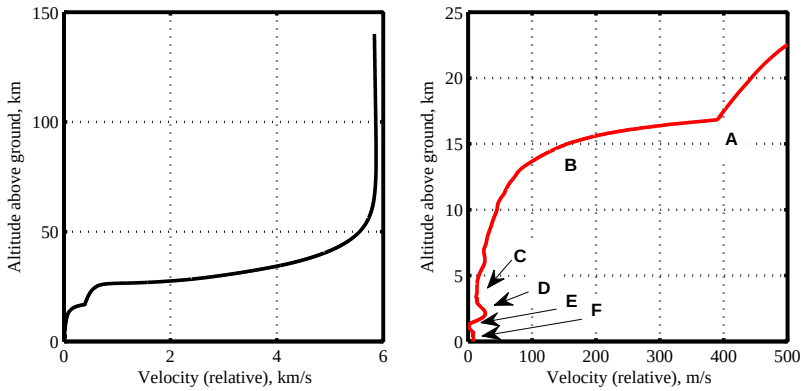

(a) Altitude vs. velocity (b) Terminal descent (zoom)

Event	Description
A	Parachute deployment
B	Heatshield separation
C	Backshell separation
D	Powered approach
E	Skycrane start
F	Touchdown sensed

(c) Events list

Figure 6. Reconstructed altitude and velocity history of MSL.

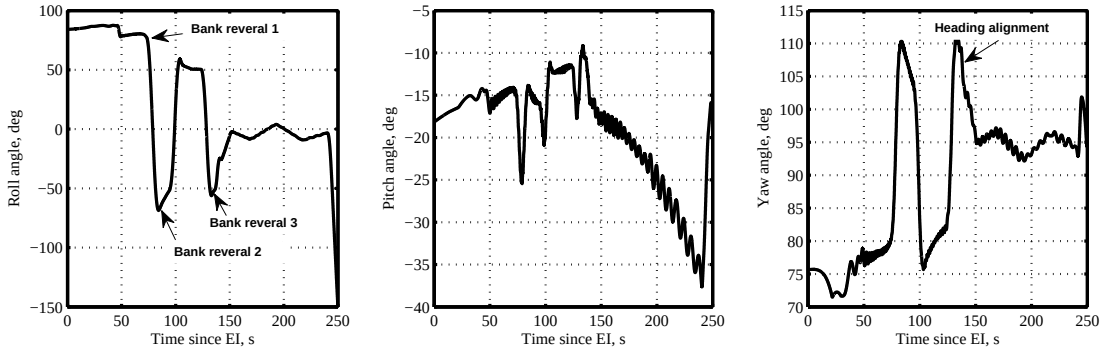

(a) Roll angle (b) Pitch angle (c) Yaw angle

Figure 7. Reconstructed attitude history of MSL.

descent phase. Parachute deployment occurs around 260 s after EI, resulting in an inflection point in the trajectory plot, while the heatshield jettison approximately 20 s after the parachute deployment results in the vehicle attaining a steady velocity. The next set of major events happen very quickly starting with the backshell separation at 375 s, powered approach at 378 s, and Sky Crane starts at 413 s. Finally, touchdown is sensed around 430 s (7 min, 10 s) after EI.

The time histories of the Euler angles - roll, pitch, and yaw - are shown in Fig. 7. Some crucial EDL events, such as bank reversals and heading alignment can be clearly seen in these figures. The bank reversals are especially interesting since MSL was the first Mars EDL vehicle that used hypersonic guidance via bank angle modulation.[1] These modulations can be clearly seen in the roll and yaw angle history. Heading alignment prior to parachute deployment is also observed in the figures. The Euler angle plots have been restricted to shortly before parachute deployment, since these angles wildly oscillate after that point.

The flight-path angle and azimuth angle relative to the planet are shown in Fig. 8. The time histories of these quantities are steady throughout the hypersonic and supersonic stages of flight, and show oscillations near the terminal descent portion when the Sky Crane was maneuvering.

The angle of attack and sideslip angle histories are shown in Fig. 9. The time axes are restricted

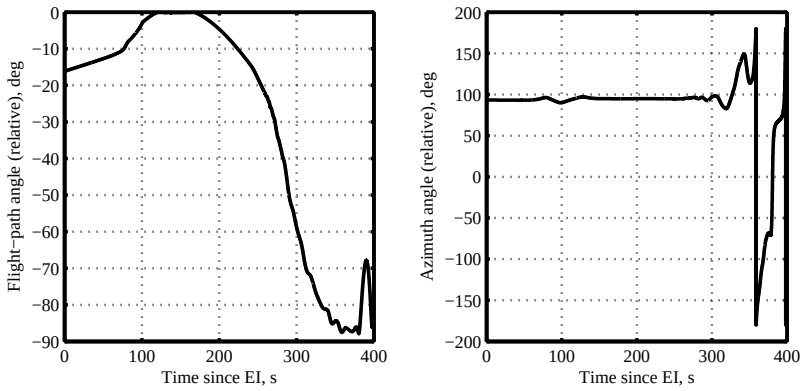

(a) Flight-path angle (b) Azimuth angle

Figure 8. Reconstructed flight-path and azimuth angle history of MSL.

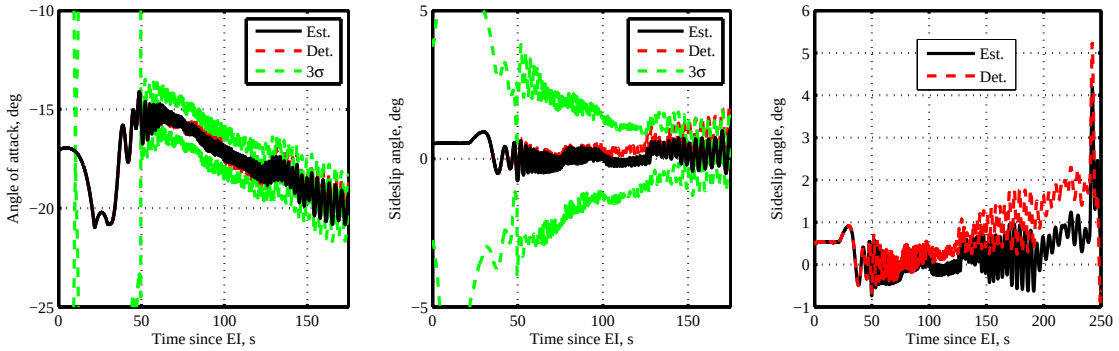

(a) Angle of attack angle (MEADS region) (b) Sideslip angle (MEADS region) (c) Sideslip angle

Figure 9. Reconstructed angle of attack and sideslip angle history of MSL. Statistically estimated (Est.) angles, deterministically estimated (Det.) angles, and statistically calculated uncertainties are shown.

from EI for Figs. 9(a) and 9(b) to the point where MEADS data was no longer processed by the estimator to show the region where the orientation angles were influenced by both IMU and FADS data. This region is also the only place in the reconstruction where aerodynamic and atmospheric uncertainties are not confounded since two independent measurements were used to estimate the angles.

One can see that the introduction of MEADS data around 50 s drastically improves the estimate of the uncertainty in Figs. 9(a) and 9(b). The deterministic reconstruction of angle of attack and sideslip angle that were only calculated using IMU data are also shown. One can see a noticeable difference between the statistically estimated (Est.) and deterministically estimated (Det.) quantities especially after 125 s in the sideslip angle plots (Figs. 9(b) and 9(c)). There is a noticeable positive bias in the sideslip angle estimate for the deterministic reconstruction and the bias also appears in the statistical estimation after MEADS data is no longer processed after 175 s. It is possible that the vehicle did indeed experience a non-zero sideslip angle, but more likely this can be explained by a significant cross wind.[11,29] Schoenenberger et al.[29] actually inferred from data that this non-zero

Table 3. Final landing location of MSL

State	Actual[30]	Reconstructed	Est. Std. Dev. (3σ)
Radius (centric), km	3391.133	3390.741	0.6048
Latitude (centric), deg	-4.5895	-4.6322	0.0752
Longitude (East), deg	137.4417	137.3940	0.0264

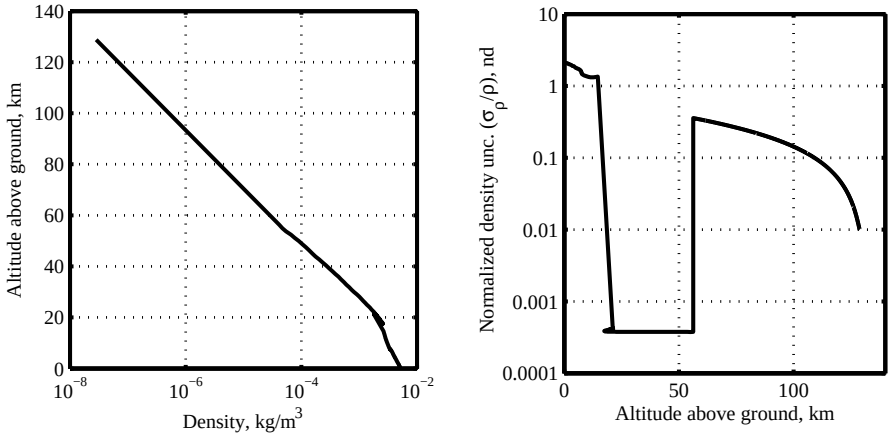

(a) Freestream density (b) Density uncertainty

Figure 10. Reconstructed atmospheric density history of MSL.

sideslip angle is actually a crab angle the vehicle sees to continue to track towards the target. Since the methodology in this paper does not estimate wind and uses the planet-relative velocity instead of the wind-relative velocity for the angle calculations, a relative strong wind may greatly affect the accuracy of the angular estimates.

The final landing location of MSL was available from post-flight communications between the rover and orbiting spacecraft.[30] This location and the reconstructed location using the estimation methodology are compared in Table 3. Although the reconstructed position is not exactly the same, the uncertainty bounds of the reconstructed position encompass the independently estimated location.

Atmosphere Estimation

One of the unique features of the estimation methodology discussed above is that atmospheric parameters are already included in the estimation state vector. Thus, there is no need to use the force coefficient equations or the hydrostatic equation to calculate atmospheric parameters. Additionally, since the accelerometer data are treated as measurements instead of part of the process equations in the estimation method, atmospheric density and pressure can be estimated with or without FADS data.

Figure 10 shows the estimated atmospheric density history as well as the estimated uncertainty. Not surprisingly, the estimated atmospheric density has a high uncertainty at the top of the atmosphere and during the terminal descent stage, two regions where MEADS data was not processed.

Freestream pressure is also an element of the state vector and is shown in Fig. 11. The freestream temperature, which was calculated using the reconstructed freestream density, freestream pressure,

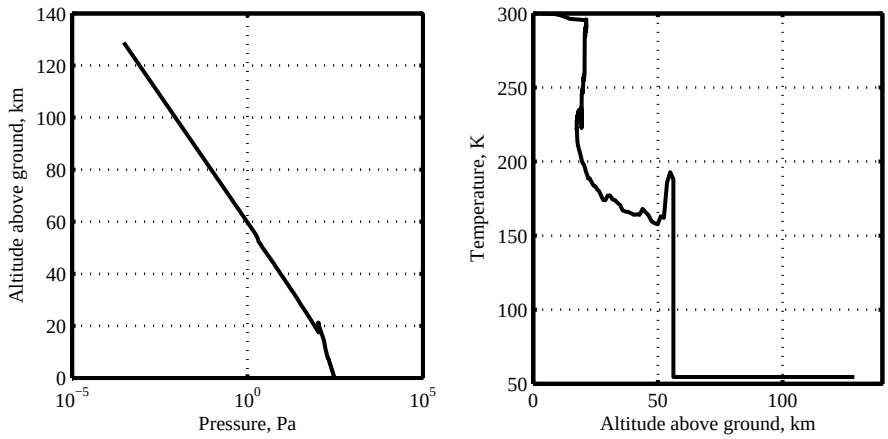

(a) Freestream pressure (b) Freestream temperature

Figure 11. Reconstructed atmospheric pressure and temperature experienced by MSL.

and the perfect gas law, is also shown in the figure. Note that the estimated freestream temperature is constant from the top of the atmosphere to the point where MEADS data is introduced. This is non-physical but completely expected with the estimation formulation, since the isothermal assumption was made in constructing dynamical equations for freestream pressure and density. Before MEADS data is introduced, pressure and temperature are related to density using the isothermal assumption of the hydrostatic equation. Density is estimated using accelerometer data only in this region, and since there are not enough independent measurements that observe all of the atmospheric parameters of interest in this region, the estimated temperature remains constant (isothermal).

The reconstructed dynamic pressure and Mach number are shown in Fig. 12. Dynamic pressure is calculated using the freestream pressure and planet-relative velocity, both quantities that are estimated by the methodology. Wind-relative velocity should be substituted for the planet-relative velocity for more accuracy, but this estimation methodology did not have means of estimating wind. Future work is planned in leveraging the estimation method to reconstruct atmospheric winds. Mach number was calculated using the planet-relative velocity and speed of sound calculated from freestream density and pressure (definition of speed of sound). However, the uncertainties in freestream pressure and density before MEADS data is introduced is also present in the speed of sound calculation, making Mach number estimates in this region highly uncertain.

CONCLUSIONS

The Mars Science Laboratory mission demonstrated the first use of hypersonic guidance for Mars entry vehicles, and the aeroshell and supersonic parachute used by the spacecraft were the largest ever flown for Martian missions. Despite the challenges, the spacecraft safely landed on Aug. 5, 2012 in Gale Crater and relayed back inertial measurement unit data, radar altimeter measurements, and flush atmospheric data system pressure measurements that provide one of the most comprehensive dataset for Mars entry vehicles.

This paper summarizes a statistical estimation methodology to reconstruct Mars Science Laboratory's trajectory and atmospheric parameters. The methodology utilizes all of the data types in one procedure and estimates states and their uncertainties while taking into account initial state and

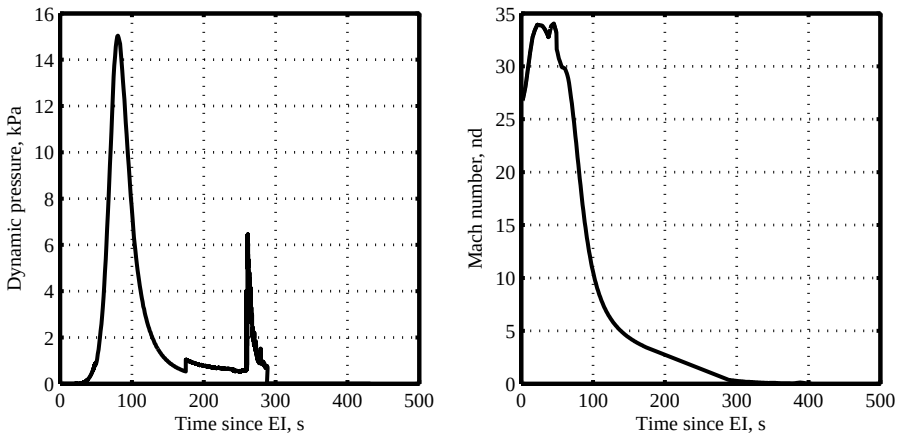

(a) Dynamic pressure (b) Mach number

Figure 12. Reconstructed dynamic pressure and Mach number history of MSL.

measurement uncertainties. The estimation state includes both trajectory and atmospheric parameters, which further leverages the coupling between the two types of parameters in the reconstruction process. A preliminary reconstruction of the Mars Science Laboratory trajectory and atmospheric parameters is presented here. The estimated quantities appear to be near nominal, and in the few instances where independent estimates are available - such as the final landing site - the estimated quantities seem close to actual results.

The work presented here uses a statistical reconstruction framework with extended Kalman filter as the estimation method. Work by the authors has shown that replacing the extended Kalman filter with unscented Kalman filter or adaptive filters can improve the estimation performance, especially the uncertainty quantification.[4,31] Future work will include re-evaluation of the MSL dataset with such estimation methods and comparison with the results presented in this paper.

ACKNOWLEDGMENT

This work was funded by a NASA Research Announcement (NRA) award (No. NNX12AF94A) and the grant's point of contact was Bernie Laub of NASA Ames Research Center. The authors would like to thank Mark Schoenenberger of NASA Langley Research Center and Chris Karlgaard of Analytical Mechanics Associates, Inc. for their advice and help in the reconstruction process.

REFERENCES

[1] A. Steltzner, D. Kipp, A. Chen, D. Burkhart, C. Guernsey, G. Mendeck, R. Mitcheltree, R. Powell, T. Rivellini, M. S. Martin, and D. Way, "Mars Science Laboratory Entry, Descent, and Landing System," IEEEAC 1497, *IEEE Aerospace Conference,* Big Sky, MT, 2006.

[2] M. P. Golombek, J. Grant, D. Kipp, and e. al., "Selection of the Mars Science Laboratory Landing Site," *Space Science Review*, July 2012, 10.1007/s11214-012-9916-y.

[3] M. J. Gazarik, M. J. Wright, A. Little, F. M. Cheatwood, J. A. Herath, M. M. Munk, F. J. Novak, and E. R. Martinez, "Overview of the MEDLI Project," IEEEAC 1510, *IEEE Aerospace Conference,* Big Sky, MT, 2008, 10.1109/AERO.2008.4526285.

[4] S. Dutta, R. D. Braun, R. P. Russell, I. G. Clark, and S. A. Striepe, "Comparison of Statistical Estimation Techniques for Mars Entry, Descent, and Landing Reconstruction from MEDLI- like Data Sources," AIAA 2012-0400, *AIAA Aerospace Sciences Meeting,* Nashville, TN, 2012.

[5] J. Christian, A. Verges, and R. Braun, "Statistical Reconstruction of Mars Entry, Descent, and Landing Trajectories and Atmospheric Profiles," AIAA 2007-6192, *AIAA SPACE Conference and Exposition,* Long Beach, CA, 2007.

[6] G. Wells and R. D. Braun, "Reconstruction of the Spirit Mars Exploration Rover Entry, Descent and Landing Performance," AA 3-2008-16, *International ARA Days Conference,* Arachon, France, 2008.

[7] S. Dutta, I. Clark, R. Russell, and R. Braun, "Statistical Entry, Descent, and Landing Performance Reconstruction of the Mars Phoenix Lander," *International Planetary Probe Workshop, Portsmouth, VA*, 2011.

[8] M. Schoenenberger, A. A. Dyakonov, P. Buning, W. Scallion, and J. Van Norman, "Aerodynamic Challenges for the Mars Science Laboratory Entry, Descent and Landing," AIAA 2009-3914, *AIAA Thermophysics Conference,* San Antonio, TX, 2009.

[9] R. D. Braun and R. M. Manning, "Mars Exploration Entry, Descent, and Landing Challenges," *Journal of Spacecraft and Rockets*, Vol. 44, No. 2, 2007, pp. 310–323, 10.2514/1.25116.

[10] A. Vasavada, A. Chen, J. Barnes, P. Burkhard, B. Canton, A. Dwyer-Cianciolo, R. Fergason, D. Hinson, H. Justh, D. Kass, S. Lewis, M. Mischna, J. Murphy, S. Rakfin, D. Tyler, and P. Withers, "Assessment of Environments for Mars Science Laboratory Entry, Descent, and Surface Operations," *Space Science Review*, 2012, 10.1007/s11214-012-9911-3.

[11] D. W. Way, D. Davis, Jody, and J. D. Shidner, "Assessment of the Mars Science Laboratory Entry, Descent, and Landing Simulation," AAS 13-420*, AAS/AIAA Space Flight Mechanics Conference, Kauai, HI*, 2013.

[12] M. Munk, A. Little, C. Kuhl, D. Bose, and J. Santos, "The Mars Science Laboratory (MSL) Entry, Descent and Landing Instrumentation (MEDLI) Hardware," AAS 13-310*, AAS/AIAA Space Flight Mechanics Conference, Kauai, HI*, 2013.

[13] K. T. Edquist, A. A. Dyakonov, M. J. Wright, and C. Y. Tang, "Aerothermodynamic Design of the Mars Science Laboratory Heatshield," AIAA 2009-4075, *AIAA Thermophysics Conference,* San Antonio, TX, 2009.

[14] J. Essmiller, P. Brugarolas, and M. San Martin, "MSL EDL GN&C Reference Frames," MSL Reconstruction TIM, Sept. 2012.

[15] C. Karlgaard, P. Kutty, M. Schoenenberger, J. Shidner, and M. Munk, "Mars Entry Atmospheric Data System Trajectory Reconstruction Algorithms and Flight Results," AIAA 2013-0028*, 51st AIAA Aerospace Sciences Meeting, Grapevine, TX*, 2013.

[16] C. D. Karlgaard, R. E. Beck, S. A. Keefe, P. M. Siemers, B. A. White, W. C. Engelund, and M. M. Munk, "Mars Entry Atmospheric Data System Modeling and Algorithm Development," AIAA 2009-3916, *AIAA Thermophysics Conference,* San Antonio, TX, 2009.

[17] N. Vinh, A. Busemann, and R. Culp, *Hypersonic and Planetary Entry Flight Mechanics*. Ann Arbor, MI: The University of Michigan Press, 1980.

[18] J. Kuipers, *Quaternions and Rotation Sequences*. Princeton, NJ: Princeton University Press, 1999.

[19] A. A. Dyakonov, M. Schoenenberger, and J. Van Norman, "Hypersonic and Supersonic Static Aerodynamics of Mars Science Laboratory Entry Vehicle," AIAA 2012-2999*, 43rd Thermophysics Conference, New Orleans, LA*, 2012.

[20] S. Dutta and R. Braun, "Mars Entry, Descent, and Landing Trajectory and Atmosphere Reconstruction," AIAA 2010-1210, *AIAA Aerospace Sciences Meeting,* Orlando, FL, 2010.

[21] B. D. Tapley, B. Schutz, and G. Born, *Statistical Orbit Determination*. Burlington, MA: Elsevier Academic Press, 2004.

[22] P. Zarchan and H. Musoff, *Fundamentals of Kalman Filtering, A Practical Approach*. Reston, VA: American Institute of Aeronautics and Astronautics, 2000.

[23] J. A. Christian, "Statistical Reconstruction of Mars Entry, Descent, and Landing Trajectories and Atmospheric Profiles," Master's thesis, Georgia Institute of Technology, 2007.

[24] D. C. Fraser and J. E. Potter, "The Optimum Linear Smoother as a Combination of Two Optimum Linear Filters," *IEEE Transactions on Automatic Control*, Vol. August, No. 31, 1969, pp. 387–390.

[25] B. Bell, "The Iterated Kalman Smoother as a Gauss-Newton Method," *SIAM Journal on Optimization*, Vol. 4, No. 3, 1994, pp. 626–636.

[26] D. Spencer, R. Blanchard, R. Braun, P. Kallemeyn, and S. Thurman, "Mars Pathfinder Entry, Descent, and Landing Reconstruction," *Journal of Spacecraft and Rockets*, Vol. 36, No. 3, 1999, pp. 348–356.

[27] R. C. Blanchard, "Entry, Descent, and Landing Trajectory and Atmosphere Reconstruction for the Mars Exploration Rovers Missions A and B," tech. rep., NASA-JPL Subcontract CCNS20568F, 2008.

[28] P. N. Desai, J. L. Prince, E. M. Queen, M. Schoenenberger, J. R. Cruz, and M. R. Grover, "Entry, Descent, and Landing Performance of the Mars Phoenix Lander," *Journal of Spacecraft and Rockets*, Vol. 48, No. 5, 2011, pp. 798–808, 10.2514/1.48239.

[29] M. Schoenenberger, J. Van Norman, A. A. Dyakonov, C. Karlgaard, D. Way, and P. Kutty, "Assessment of the Reconstructed Aerodynamics of the Mars Science Laboratory Entry Vehicle," AAS 12-306*, AAS/AIAA Space Flight Mechanics Conference, Kauai, HI*, 2013.

[30] C. Karlgaard, P. Kutty, M. Schoenenberger, and J. Shidner, "Mars Science Laboratory Entry, Descent, and Landing Trajectory and Atmosphere Reconstruction," AAS 13-307*, AAS/AIAA Space Flight Mechanics Conference, Kauai, HI*, 2013.

[31] S. Dutta, R. Braun, and C. Karlgaard, "Uncertainty Quantification for Mars Entry, Descent, and Landing Reconstruction Using Adaptive Filtering," AIAA 2013-0026*, 51st AIAA Aerospace Sciences Meeting, Grapevine, TX*, 2013.